LAWRENCE
LIVERMORE
NATIONAL
LABORATORY

LLNL-PROC-412857

Cyclotron Resonances in Electron Cloud Dynamics

C. M. Celata, M. A. Furman, J- L. Vay, D. P. Grote, J. S. T. Ng, M. T. F. Pivi, L. F. Wang

May 7, 2009

PAC2009
Vancouver, Canada
May 4, 2009 through May 8, 2009

Disclaimer

CYCLOTRON RESONANCES IN ELECTRON CLOUD DYNAMICS*

C. M. Celata#, Miguel A. Furman, J.-L. Vay, LBNL, Berkeley, California U.S.A.
D. P. Grote, LLNL, Livermore, California U.S.A.
J. S.T. Ng, M. T. F. Pivi, L. F. Wang, SLAC, Menlo Park, California U.S.A.

Abstract

A new set of resonances for electron cloud dynamics in the presence of a magnetic field has been found. For short beam bunch lengths and low magnetic fields where $l_b << 2\pi\omega_c$, (l_b = bunch duration, ω_c = non-relativistic cyclotron frequency) resonances between the bunch frequency and harmonics of the cyclotron frequency cause an increase in the electron cloud density in narrow ranges of magnetic field near the resonances. For ILC parameters the increase in the density is up to a factor ≈ 3, and the spatial distribution of the electrons is broader near resonances, lacking the well-defined density "stripes" of multipactoring found for non-resonant cases. Simulations with the 2D computer code POSINST, as well as a single-particle tracking code, were used to elucidate the physics of the dynamics. The resonances are expected to affect the electron cloud dynamics in the fringe fields of conventional lattice magnets and in wigglers, where the magnetic fields are low. Results of the simulations, the reason for the bunch-length dependence, and details of the dynamics will be discussed.

INTRODUCTION

Because of high bunch intensity and frequency, electron cloud effects are an important design issue in modern high-energy accelerators with intense beams of positive charge, as well as in lower-energy accelerators of intense ion beams. As an example, in the International Linear Collider (ILC) bending of the beam in the positron damping ring will produce copious synchrotron radiation. This then will generate photoelectrons, which in turn create secondaries. The resultant electron cloud is expected to cause emittance growth and beam instability, limiting the average beam current. To quantify the cloud density and distribution for ILC damping ring parameters, a series of computer simulations was done with the 2D computer code POSINST [1]. Of interest is the area of the wiggler, where the magnetic field varies from zero to about 2 T. Results showed that above a certain threshold in magnetic field magnitude, B, the cloud density calculated was a smooth function of B. Below this threshold there were large (x3) increases in the density over very narrow ranges of B which had a strict periodicity. This paper discusses and explains this enhancement of the electron cloud density and shows that it is due to resonances between the beam passage and the electron cyclotron frequency.

*Work supported by Office of Science, U. S. D.O.E, Contract No. DE-AC02-05CH11231 and LLNL contract DE-AC52-07NA27344.
#Present affiliation: Cornell University, Ithaca, NY, U.S.A., and visitor at California Institute of Technology, Pasadena, CA USA

SIMULATION MODEL

Since POSINST is a 2D code, in order to simulate the wiggler a series of runs was done where each run approximated a transverse slice of the wiggler as a dipole ($B_x=B_z=0$, B_y constant). Photon reflectivity was assumed to be unity—i.e., photoelectrons were formed in a distribution uniform in azimuthal angle. Since the electrons are tied to field lines and therefore only sample a limited region in x, this choice of reflectivity permitted investigation of the dynamics at all x. The physical and numerical parameters used in the simulations are shown in Table 1.

The beam bunch density was assumed to be Gaussian in x,y, and z and centered in the circular vacuum chamber. The centroid motion due to the wiggler field was not included in the model. The bunch distribution was not allowed to evolve during the simulation. It is assumed that such evolution is negligible during the few microseconds of the cloud buildup. All electrons were assumed to be formed either by photoionization or by secondary emission due to wall impact of the photoelectrons—ionization of background gas was assumed to be negligible. Further details of the model and results not shown here can be found in ref. [2].

Table 1: Parameters for all Simulations

Bunch spacing, τ_b	6.15 ns
σ_x (beam)	112 μm
σ_y (beam)	4.6 μm
σ_z (beam)	6.0 mm
Full bunch length	±2.5 σ_z
Photons emitted per positron per meter	0.07
Quantum efficiency	0.1
Peak secondary electron yield at normal incidence	1.4
PIC spatial grid cell size	0.36 mm
Integration Time Step	1.25×10^{-11} s
Vacuum pipe radius, a	2.3 cm

SIMULATION RESULTS

As beam bunches pass a given location in the damping ring, the electron cloud builds up until the loss of electrons due to electron space charge repulsion balances their production, thus attaining an equilibrium value. Figure 1 shows the "equilibrium average density" for the electron cloud as a function of $n \equiv \omega_c/\omega_b$, where ω_c is the nonrelativistic electron cyclotron frequency and $\omega_b=2\pi/\tau_\beta$,

where τ_β is the time interval between passages of successive bunch centers. Thus n∝B. The equilibrium average density is the total number of electrons at equilibrium in the chamber divided by the chamber volumey. Note that the "+" marks on the figure denote simulation results. Lines are only provided to guide the eye. A horizontal expansion of this graph shows that all peaks are at integral multiples of n, and at every integral value of n where a run was done the density was enhanced. Thus, if more runs had been done the peaks would be seen to be evenly spaced in n—areas where the peaks seem to be sparser simply reflect the fact that simulations were not done to outline all 100 peaks.

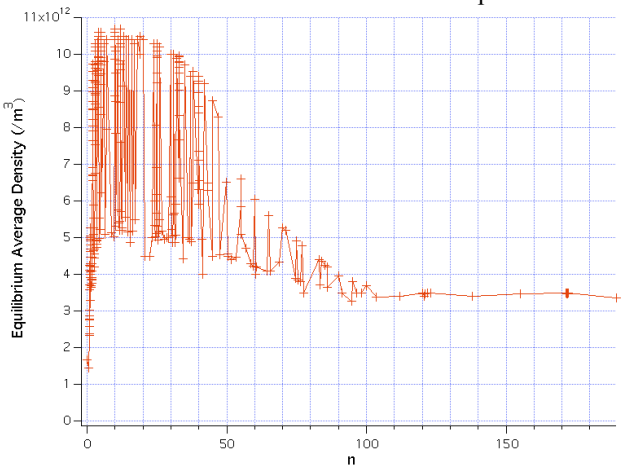

Figure 1: Equilibrium average density vs. n

The spatial distribution of electrons is different at B values where the density is enhanced. Figure 2 shows the density as a function of x and y for B=0.07 T (n=12) and B=0.08 T (n=13.8). The density shown in the figure is integrated over the full time of the simulation, but since most of the simulation is spent during the equilibrium phase, it is weighted heavily toward this phase. At n=13.8 the well-known vertical stripes of high-density are seen. These form where the kick from the beam gives electrons an energy which is near the peak of the function giving secondary electron yield vs. energy [3]. But at n=12 the electrons are much more evenly distributed. Thus, depending on photon reflectivity, at magnetic field values where n is integral the effect of the electron cloud on the beam and the power deposition by the electrons at the wall can be quite different from the well-known picture at nonintegral n.

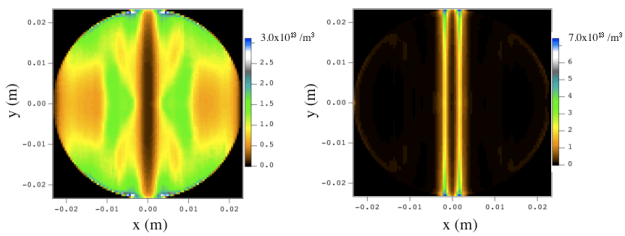

Figure 2: Density distribution for a resonant (0.07T) and non-resonant (0.08T) case. Vacuum chamber is circular and fits exactly within the plot.

The fact that the electron density enhancement occurs when the cyclotron frequency is an integral multiple of the bunch frequency suggests that the increased density is due to a resonance between the appearance of the bunch and the position of an electron in its cyclotron orbit. Since the magnetic field is uniform in this problem, all electrons in the system have the same cyclotron frequency, unless they acquire enough energy for a non-negligible relativistic mass increase. Simulation data shows that such a mass increase occurs only for a very small fraction of the electron population. For the rest, then, each time the beam appears the electron will be at the same position in its cyclotron orbit. Note that for low B, in the range of the highest density peaks in Fig. 1, the time for the beam to pass an electron is much less than the cyclotron period, i.e.,

$$B << 2\pi \frac{m_e c}{e l_b} \qquad (1)$$

where l_b is the bunch length, c is the speed of light, and m_e is the electron mass. Thus the electron experiences the force of the beam as essentially an instantaneous kick at one point in its gyro-orbit. The beam force is in the x-y plane-- z forces are neglible because the beam velocity is approximately c. The y force accelerates the electron vertically, i.e., parallel to the magnetic field. The force in the x direction accelerates the electron in the plane of its cyclotron gyration, the x-z plane. The direction of this force is toward the y axis so it will rotate the perpendicular (to B) component of the electron velocity toward this direction. For the case of an intense beam like the ILC beam, it only requires a few kicks to align the electron velocity at the time of the bunch passages with the x component of the bunch electric field, after which the kick of each bunch will simply increase the perpendicular velocity. The effect of the resonance, then, is to synchronize the phases of the electrons in their cyclotron motion, increase the perpendicular energy of the electrons, and thereby also increase the angle (to the normal of the surface) with which electrons hit the chamber wall as they travel along the B field lines. The dependence of the secondary electron yield on the impact energy and angle is shown in Fig. 3. From this it can be seen that both the increase in energy and the increase in the angle to the surface normal will increase the yield of secondary electrons. This accounts for the density spikes of Fig. 1. Figure 4 displays POSINST results showing the difference in electron energy spectrum and spectrum of the cosine of the impact angle for cases of B on and off resonance.

Calculations without electron space charge were done to demonstrate the electron dynamics in a simpler system. The force of the beam was approximated by an instantaneous kick. For resonant B values results did indeed show the phases of the electrons in their gyro-orbits at the time of the bunches' arrival converging over time to lock into a direction parallel to the x component of

the beam force. The electron perpendicular energy increased, causing an increase in the mass and detuning of the gyrophase. However this detuning occurred after several bunch passage times, by which time all but a few electrons had left the system. In all respects the single particle calculations confirmed the description above of the dynamics of the resonance.

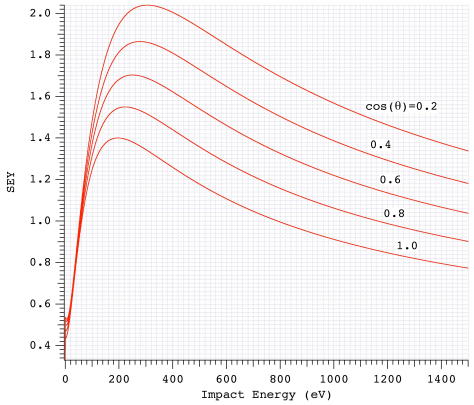

Figure 3: Secondary electron yield vs. electron impact energy and angle to the surface normal for our parameters

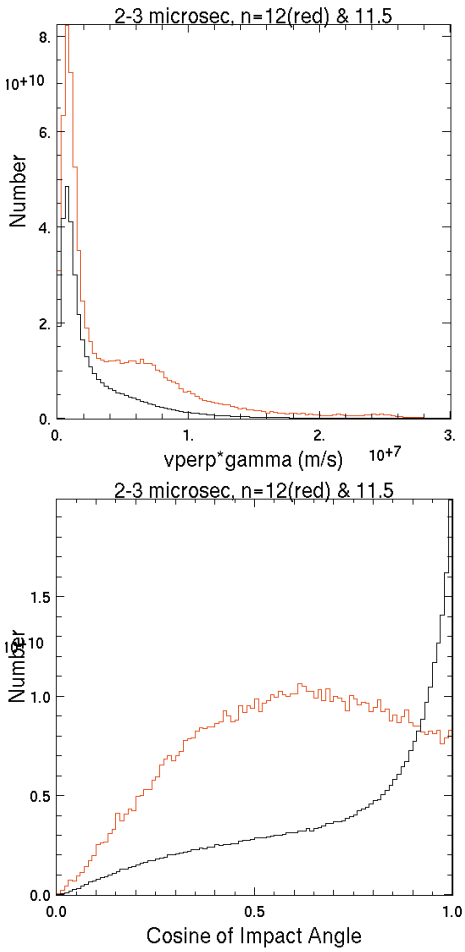

Figure 4: Spectra of impact energy and angle to the surface normal of electrons hitting the wall during cloud buildup for n=12 (red) and n=11 (black).

As the magnetic field increases, the cyclotron frequency increases, and Eq. (1) is no longer valid. The beam force now occurs over a significant portion of the cyclotron period. Since the electron velocity is changing direction during the beam passage, the electron will be both accelerated and decelerated during that time, so that much of the effect of the beam in the perpendicular direction is cancelled. This is the cause of the decrease of the density peak amplitude with increasing B in Fig. 1.

Finally, we note that at low n the density peaks have a complicated structure, with a minimum near integral n, which disappears as n increases. This is shown in Fig. 5. Electron statistics for a case near peak density at n=1.93 were compared to those at n=2 in order to clarify the dynamics at low n. The cloud buildup in both cases was similar, diverging only after space charge was significant. The presence of space charge made it difficult to see a simple explanation for the difference. We do note, however, that electrons at n=2 on average stay in the system longer than those at n=1.93. They thus attain higher energy. But at n=1.93 the shorter confinement time of the electrons in the system, and thus higher impact rate at the wall, more than compensates for somewhat lower impact energy so that more secondary electrons were produced. Though the difference of confinement time accounts for the decline in cloud density at the resonance, we have no theory at this time which explains the longevity of electrons at different B field values.

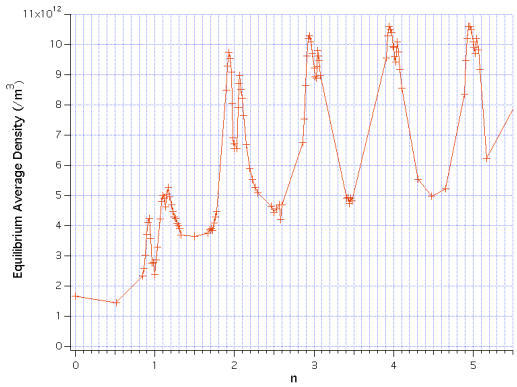

Figure 5: Equilibrium average density vs. n for low n.

ANALYTICAL MODEL

A simplified analytical model of the electron dynamics can be used to derive many of the characteristics of the electron motion described above. We make the following assumptions: (1) the electrons remain non-relativistic, even at resonance, (2) space-charge forces and image forces from the vacuum chamber are neglected, (3) electron cyclotron radius << chamber radius, (4) $\sigma_t << 2\pi/\omega_b$, where σ_t is the RMS bunch duration; (5) we do not include electron motion which impacts the chamber walls, and (6) we restrict our attention to only those electrons with small vertical amplitude. The line charge density of the positron beam at time t and longitudinal location z is given by

$$\lambda(z,t) = eN_b \sum_{k=0}^{\infty} \frac{e^{-(z-ct+kc\tau_b)^2/(2\sigma_z^2)}}{\sqrt{2\pi}\,\sigma_z} \qquad (2)$$

where the summation is over successive bunches. While in a real accelerator the number of bunches is finite, the infinite upper limit in the above summation does not affect the results in the analysis that follows.

The electric field generated by the beam is

$$\mathbf{E}(x,y,z,t) = \frac{\lambda(z,t)}{4\pi\varepsilon_0}\mathbf{G}(x,y) \qquad (3)$$

where $\mathbf{G}(x,y)$, with dimensions of 1/length, is the 2-dimensional Bassetti-Erskine field. The magnetic field **B** has an external component $\mathbf{B}=\mathrm{B}\,\hat{y}$ plus the contribution generated by the beam, $\mathbf{B_b} \approx -\hat{z} \times \mathbf{E}/c$. The contribution from this latter component to the $\mathbf{v}\times\mathbf{B}$ force is at most $e\beta E$ (where $\beta=v/c$), hence down by a factor of v/c relative to the electric force, hence negligible in magnitude compared to **E**. Very near to the beam, especially for low values of the dipole field, the magnetic field of the beam will change the direction of the B field for the short time that a bunch is present. This effect is not present in the POSINST calculations or in this analysis, and will be explored in future work.

We first solve the equations of motion neglecting the field from the beam. The equations are then

$$\begin{aligned} \dot{v}_x &= \omega v_z \\ \dot{v}_y &= 0 \\ \dot{v}_z &= -\omega v_x \end{aligned} \qquad (4)$$

where $\omega=eB/m_e$. The solution in the x-z plane is

$$\begin{aligned} v_{f,z} &= -\omega\rho_0 \sin(\omega t + \phi_0) \\ v_{f,x} &= +\omega\rho_0 \cos(\omega t + \phi_0) \end{aligned} \qquad (5)$$

where the subscript "f" stands for "free" (i.e., in the absence of the beam). The gyroradius ρ_0 is determined by the initial condition, $\omega\rho_0 = v_{\perp 0}$, where $v_{\perp 0}$ is the initial speed in the x-z plane; ϕ_0 is the initial phase. The solutions for x and z are:

$$\begin{aligned} z_f(t) &= z_c + \rho_0 \cos(\omega t + \phi_0) \\ x_f(t) &= x_c + \rho_0 \sin(\omega t + \phi_0) \end{aligned} \qquad (6)$$

where $(z_c,x_c) = (z_{f,0} - v_{f,x0}/\omega,\ x_{f,z0} + v_{f,z0}/\omega)$ is the gyrocenter in the (x-z) plane expressed in terms of the components of the velocity at t=0. As for the motion in y, it is free-particle motion: $v_y=v_{y0}$ and $y=y_0+v_{y0}t$.

From the original equations of motion we have:

$$\begin{aligned} \ddot{v}_z + \omega^2 v_z &= \frac{\omega^2 E_x}{B} \\ &= \frac{eN_b\omega^2 G_x(x,y)}{4\pi\varepsilon_0 B} \sum_{k=0}^{\infty} \frac{e^{-(z-ct+kc\tau_b)^2/(2\sigma_z^2)}}{\sqrt{2\pi}\,\sigma_z} \end{aligned} \qquad (7)$$

Under our stated assumptions we can derive an approximation to this equation by setting x, y and z in the right-hand side to their values at t=0, keeping only the essential time dependence in the exponential factor. Without any loss of generality we choose z_0=0, hence

$$\ddot{v}_z + \omega^2 v_z \approx \frac{eN_b\omega^2 G_x(x_0,y_0)}{4\pi\varepsilon_0 Bc} \sum_{k=0}^{\infty} \frac{e^{-(t-k\tau_b)^2/(2\sigma_t^2)}}{\sqrt{2\pi}\,\sigma_t} \qquad (8)$$

which is the equation for a driven harmonic oscillator. We readily find $v_z = v_{f,z}(t) + v_{d,z}(t)$, where the free part, v_f, is given by Eq. (8) and the driven part is given by

$$v_{d,z}(t) = \theta(t)\kappa N_b r_e c\, G_x(x_0,y_0)\, A(K,n) \sin\xi \qquad (9)$$

where $\theta(t)$ is the conventional step function, $\kappa = e^{-(\omega\sigma_t)^2/2}$, K is the largest integer $\le t/\tau_b$, $n=\omega\tau_b/2\pi$, $r_e = e^2/(4\pi\varepsilon_0 m_e c^2) \approx 2.82\times10^{-15}$ m is the classical radius of the electron, $\xi=\omega t-\pi nK$, and the amplitude A is given by

$$A(K,n) = \frac{\sin(\pi n(K+1))}{\sin(\pi n)}. \qquad (10)$$

To complete the derivation we note that $m_e\dot{v}_z = -eB\dot{x}$, hence $x(t) = x_0 - (v_z(t)-v_{z0})/\omega$. We obtain $v_x(t) = v_{f,x}(t)+v_{d,x}(t)$, where

$$v_{d,x}(t) = \theta(t)\kappa N_b r_e c\, G_x(x_0,y_0)\, A(K,n) \cos\xi \qquad (11)$$

and $z(t) = z_f(t)+z_d(t)$ and $x(t) = x_f(t)+x_d(t)$ where the driven parts are given by

$$\begin{aligned} z_d(t) &= -\theta(t)\kappa N_b r_e c\, G_x(x_0,y_0)\, A(K,n) \cos\xi/\omega \\ x_d(t) &= +\theta(t)\kappa N_b r_e c\, G_x(x_0,y_0)\, A(K,n) \sin\xi/\omega \end{aligned} \qquad (12)$$

The 1st-order equation for motion in y can be obtained in similar fashion, but it does not add much useful information to the discussion. One finds that those electrons for which the x component of the gyrocenter, x_c, is comparable to or slightly smaller than the chamber radius a oscillate harmonically about y=0 with an angular frequency

$$\omega_y \approx \sqrt{\frac{2N_b r_e c}{x_c^2 \tau_b}} \qquad (13)$$

but those electrons whose gyrocenter x_c is within ~a/2 of the pipe center (x=0) are very unstable under the action of the beam, and are driven to the wall of the chamber within one to a few bunch passages (for the parameter values in Table 1).

Equations (9), (11) and (12) are the basic result of this analysis. The amplitude $A(K,n)$ is responsible for the linear growth in time of the motion whenever $n = \omega\tau_b/2\pi$ is an integer, because in this case $|A(K,n)|=K+1$, which grows with time. Thus the driven component of the amplitude quickly dominates the motion, the initial phase ϕ_0 and amplitude $\omega\rho_0$ become irrelevant, and the phase of the horizontal velocity (Eqs. (9) and (11)) is uniquely determined by the beam driving force. One readily finds from Eqs. (9-11) also the synchronization of the electron cyclotron phase discussed in the last section. For integer n, the electron energy therefore grows like $|A|^2 \sim t^2$, explaining why in this case the electron-wall collision energy is larger than for non-integer n. Finally, if the

bunch length is too large, or the B field too strong, the resonant growth of the amplitude is suppressed by the phase-averaging factor $\kappa = e^{-(\omega\sigma_t)^2/2}$ [4].

EXPERIMENTAL OBSERVATION OF RESONANCES

An experiment in a chicane at the PEP-II positron storage ring was used to experimentally observe the cyclotron resonances. Details of the experiment can be found in ref. [5]. Each of three dipoles in the chicane was instrumented with a retarding field analyzer (RFA) located at the top of the vacuum chamber. The RFA collectors were segmented in x into 17 stripes which could be biased in order to measure the electrons' vertical kinetic energy. The vacuum wall was aluminum, but in the second dipole a TiN coating was used to decrease the secondary emission of the wall. Results are shown in Fig. 6. Increases in density can be seen which are periodic in B, and their spacing is identical to what is expected for the resonances described above. However there are complicated features not evident in the simulations. For the aluminum surface, data from the collector stripe farthest from the beam (x=29 mm) showed clear resonance peaks at the expected integer n values. Collector stripes closer to the beam axis (x = 0), showed peaks with a double-spike structure. This effect was so severe that at $x = \pm 5$ mm, the signal enhancement had shifted to half-integer values of n. This was not observed for TiN-coated surface, where resonances occurred for integer n (at large n) for all collector stripes. It is unknown at this point whether these complicated features are related to effects of the RFA or to 3D field effects or something as yet undiscovered. The chicane experiment has been moved to Cornell University and installed at CESR-TA, and experiments and analysis will continue there in order to clarify these results.

REFERENCES

[1] POSINST
[2] our PRSTAB
[3] cause of dipole stripes
[4] M. A. Furman and G. R. Lambertson, ``The Electron-Cloud Instability in PEP-II: an Update,", Proc. PAC97
[5] Pivi EPAC paper?